Development and Evaluation of a Convection Scheme for Use in Climate Models

KERRY A. EMANUEL

Program for Atmospheres, Oceans, and Climate, Massachusetts Institute of Technology, Cambridge, Massachusetts

MARINA ŽIVKOVIĆ-ROTHMAN

Atmospheric and Environmental Research, Inc., Cambridge, Massachusetts

(Manuscript received 5 January 1998, in final form 11 May 1998)

ABSTRACT

Cumulus convection is a key process in controlling the water vapor content of the atmosphere, which is in turn the largest feedback mechanism for climate change in global climate models. Yet scant attention has been paid to designing convective representations that attempt to handle water vapor with fidelity, and even less to evaluating their performance. Here the authors attempt to address this deficiency by designing a representation of cumulus convection with close attention paid to convective water fluxes and by subjecting the scheme to rigorous tests using sounding array data. The authors maintain that such tests, in which a single-column model is forced by large-scale processes measured by or inferred from the sounding data, must be carried out over a period at least as long as the radiative-subsidence timescale—about 30 days—governing the water vapor adjustment time. The authors also argue that the observed forcing must be preconditioned to guarantee integral enthalpy conservation, else errors in the single-column prediction may be falsely attributed to convective schemes.

Optimization of the new scheme's parameters is performed using one month of data from the intensive flux array operating during the Tropical Ocean Global Atmosphere Coupled Ocean–Atmosphere Response Experiment, with the aid of the adjoint of the linear tangent of the single-column model. Residual root-mean-square errors, after optimization, are about 15% in relative humidity and 1.8 K in temperature. It is difficult to reject the hypothesis that the residual errors are due to noise in the forcing. Evaluation of the convective scheme is performed using Global Atmospheric Researh Program Atlantic Tropical Experiment data. The performance of the scheme is compared to that of a few other schemes used in current climate models. It is also shown that a vertical resolution better than 50 mb in pressure is necessary for accurate prediction of atmospheric water vapor.

1. Introduction

Water vapor is the most important greenhouse substance in the atmosphere, accounting for most of the longwave absorption and a modest amount of shortwave absorption of radiation. It is also the strongest feedback factor in externally forced global climate change in all of the 19 global climate models participating in the Atmospheric Model Intercomparison Project (AMIP) as of 1990 (Cess et al. 1990). In addition to its important direct effects on radiative transfer, it is strongly associated with the distribution of stratiform clouds, which themselves have a strong influence on radiation. Understanding and predicting atmospheric water vapor is clearly of paramount importance for climate simulation and prediction.

Atmospheric water vapor content is controlled by large-scale circulation, surface fluxes, and cloud microphysical processes, as reviewed by Emanuel and Pierrehumbert (1996). As the median residence time of a water molecule in the atmosphere is about 10 days, we may assume that atmospheric water vapor is in statistical equilibrium with the rest of the climate system in the long-term average. The basic elements of the physics underlying atmospheric water vapor are illustrated schematically in Fig. 1. It is helpful to think about the circulation relative to the time-averaged position of isentropic surfaces, here denoted as surfaces of constant potential temperature (θ). In the Tropics, vertical exchange is almost entirely diabatic, with virtually all upward displacement occurring within convective clouds. Outside the Tropics, there are larger adiabatic components to (sloping) vertical displacements but even in this case much of the ascent takes place within clouds.

At any one time, only a small percentage of the volume of the troposphere resides in clouds, so to a first approximation the question of atmospheric water vapor content reduces to the question of the humidity of unsaturated air outside clouds. Consider the time history

Corresponding author address: K. A. Emanuel, Room 54-1620, Massachusetts Institute of Technology, 77 Massachusetts Avenue, Cambridge, MA 02139.
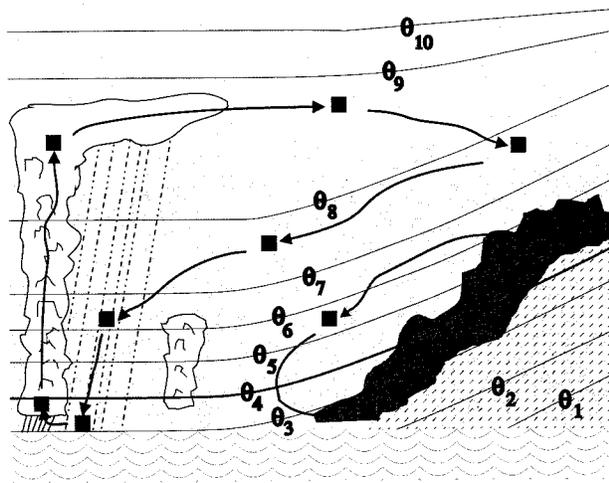E-mail: emanuel@texmex.mit.edu

FIG. 1. Control of free atmosphere water vapor by cloud processes. Diagram extends from equator (left) to high latitudes (right) and extends from surface to lower stratosphere. White clouds represent cumuli while the dark cloud represents sloping ascent in baroclinic systems. Thin solid lines are isentropic surfaces. Parcels crossing isentropic surfaces to higher values of potential temperature (θ) must do so within clouds. Parcels sinking through θ surfaces experience radiative and/or evaporative cooling. In a Lagrangian view, water vapor content of parcels sinking through the troposphere is determined by microphysical processes within clouds, which set the total water content of detraining air, by evaporation of falling precipitation and by detrainment from shallow clouds.

of water vapor mixing ratio in a test sample of air that starts out in the tropical maritime boundary layer, as illustrated in Fig. 1. The sample will eventually ascend within a convective cloud. It is readily seen that the total water content of the sample when it is detrained from the cloud will be a function of microphysical processes within the cloud, as well as turbulent entrainment. For a sample that emerges near the tropopause, the vast majority of its initial water will have been lost to precipitation, but if even a small fraction of condensed water remains in the sample, it may be far greater than the water vapor mixing ratio of its environment; thus, its value is important. From the point of view of radiative transfer, fluctuations of relative humidity in the upper troposphere can be as important as those of the lower troposphere, even though the absolute amount of water involved is tiny by comparison (Lindzen 1990).

Air detrained from cumulonimbi gradually descends across θ surfaces under the influence of radiative cooling. For a cooling rate of 1.5 K day^{-1}, it will take 20 days to descend across 30 K of potential temperature variation, typical of the change across the depth of the troposphere. But 20 days is comparable to or longer than the timescales typical of large-scale atmospheric circulation, so that individual samples typically undergo large lateral excursions during their descent. In a stochastic sense, some of the samples will be exposed to falling precipitation and detrainment from shallower clouds and will thus acquire some water vapor as they

descend; some percentage of samples may largely avoid such encounters and nearly preserve the total water content they had on emerging from deep cumulonimbi. Those parcels, by the time they descend even to 400 mb, would have extremely low relative humidity. Such small humidities have been detected (Spencer and Braswell 1997). Satellite water vapor imagery makes it clear, however, that the water vapor content of the atmosphere has large horizontal and temporal variability (Pierrehumbert and Yang 1993), and much of the cloud-free atmosphere is substantially more humid than can be explained by descent in the absence of mixing.

This exercise clearly demonstrates that atmospheric water vapor content depends strongly on microphysical processes within convective and associated stratiform clouds, and on the evaporation of precipitation. Atmospheric dynamics may modify but cannot eliminate this sensitivity. To make the point in an obvious way, if precipitation (but not cloud) were microphysically impossible, most of the atmosphere would be saturated, regardless of dynamics.

Given the expected sensitivity of climate to convective cloud microphysics, it is surprising how little attention has been paid to microphysical aspects of convective parameterizations used in global climate models. Of the 36 quasi-independent model versions now participating in the Atmospheric Model Intercomparison Project (AMIP), almost three-quarters employ one of only three different convective schemes: those of Manabe et al. (1965), Kuo (1974), and Arakawa and Schubert (1974). (In most cases, the actual schemes employed differ in some ways from the original versions of these schemes.) In the original convective adjustment scheme of Manabe et al. (1965), *all* condensed water is removed during adjustment, with no reevaporation. There are many variants of the Kuo scheme, but they generally take an extremely simple approach to the partitioning between convection moistening and precipitation, typically representing the partitioning by a single parameter. Of the 28-page description of the Arakawa–Schubert (1974) scheme, a single line in an appendix is devoted to a discussion of the microphysics of precipitation formation. More serious even than the scant attention paid to microphysics is the paucity of attempts to rigorously test against observations the fidelity of moistening produced by these schemes under controlled conditions.

Single-column models of radiative–convective equilibria indeed show great sensitivity to the way water is treated in representations of cumulus convection. Rennó et al. (1994) showed large variability in equilibrium states and climate sensitivities among various convective schemes and with variations of microphysical parameters within individual schemes.

On the other hand, the output of global climate models hardly seems to call attention to the problem of control of atmospheric water vapor. The standard deviation among the water vapor feedback factors of 19 GCMs

described by Cess et al. (1990) was a factor of 5 smaller than that owing to cloud-radiation feedback, leading the authors to recommend focusing on the representation of clouds in climate models. We shall argue, toward the conclusion of this paper, that the disparity between physical reasoning and single-column model results on the one hand, and global climate model results on the other, may be an artifact of insufficient vertical resolution in global models.

This paper is devoted to a description of a revised cumulus parameterization that focuses on the need to represent accurately both entrainment and microphysical processes, and to the construction and execution of observational tests designed to rigorously optimize and evaluate the convective scheme. We also demonstrate the sensitivity of water vapor prediction to vertical resolution and conclude with a discussion of requirements for high-quality simulation of atmospheric water vapor in climate models.

2. Design

The basis of the new convective scheme is the representation of convection described earlier by the first author (Emanuel 1991, hereafter E91). This scheme appears to perform comparably to others when run in regional weather forecasting models (Gyakum et al. 1996). It was recognized, in designing that scheme, that a good representation of convection should be consonant with important observed properties of cumulus clouds, including

(A) the ability of deep cumulonimbi to penetrate to the level of neutral buoyancy of *undilute* subcloud-layer air;

(B) notwithstanding a, the fact that the mass of a convective cloud is composed mostly of entrained air;

(C) the fact that saturated downdrafts can be as strong as updrafts in nonprecipitating cumulus clouds (Wei et al. 1998); and

(D) the fact that unsaturated downdrafts driven by evaporation of precipitation are important agents of transport and are critical for restabilizing the atmosphere to convection from the boundary layer.

Observations A and C decisively rule out the notion that convective clouds can be modeled as entraining plumes, as is done in several schemes, including that of Arakawa and Schubert (1974). The only way that entraining plumes can be made to conform to observations A and B together is to assume that the deepest plumes do not entrain at all; this is radically at odds with observations (Warner 1970). And, of course, entraining plumes cannot account for observation C at all. The plume model cannot mimic the transports of nonprecipitating cumuli, in which updrafts and downdrafts are equally important (as there is no net heating by such clouds), except by detraining condensed water from their tops and thus

concentrating the evaporative cooling there. Partially for this reason, many climate models artificially divide the spectrum of convective clouds into shallow and deep clouds and represent each by separate parameterizations. As the real spectrum of convective clouds is continuous, if bimodal, a unified treatment of the clouds is clearly desirable.

For these reasons, the scheme of E91 was based on the buoyancy-sorting hypothesis of Raymond and Blyth (1986), which is consistent with observations A and B above and with other observed properties of real clouds (Taylor and Baker 1991) and of high-resolution numerical simulations of shallow cumulus clouds (Carpenter et al. 1998). It assumes that mixing in clouds is highly episodic and inhomogeneous, rather than continuous as in the entraining plume model. Air that is mixed into a cloud from the environment is assumed to form a spectrum of mixtures of differing mixing fraction, which then ascend or descend to their respective levels of neutral buoyancy. In this respect, the present scheme is unchanged from that of E91.

The buoyancy-sorting hypothesis by itself leaves open the issue of the rate of mixing between the plume and its environment. This is one of the great unsolved problems in cumulus convection. In laboratory plumes, experiments and dimensional analysis strongly support the contention that mixing is a simple function of the mean upward velocity of the plume. But in penetrative convection, the stable stratification of the environment evidently modifies the rate of entrainment and detrainment. The present mixing formulation is loosely fashioned after the modeling work by Bretherton and Smolarkiewicz (1989), which suggests that entrainment and detrainment rates are functions of the vertical gradients of buoyancy in clouds. The fraction of the total cloud-base mass flux, M_b, that mixes with its environment at any level is given in the present scheme by

$$\frac{\delta M}{M_b} = \frac{|\delta B| + \Lambda \delta p}{\sum_{i=1}^{N} [|\delta B| + \Lambda \delta p]}. \quad (1)$$

Here δM is the rate of mixing of undilute cloud air, M_b is the net upward mass flux through cloud base, Λ is a mixing parameter, B is the buoyancy of undilute cloud air, δB is the change in undilute buoyancy over a pressure interval δp, and N is the number of model levels. As described later, the mixing δM can result in either entrainment or detrainment, according to the buoyancy of the mixtures. The absolute value operation in (1) reflects this fact: increasing buoyancy with height can be expected to enhance entrainment while decreasing buoyancy enhances detrainment; either increases the rate of mixing as it is defined here. The formulation (1) allows cloud mass fluxes to adjust to cloud buoyancy and thus to drive the system rapidly toward quasi equilibrium.

The buoyancy-sorting hypothesis (as described in de-

tail in E91) together with the mixing hypothesis [(1)] determine the net mass flux, given the net upward mass flux M_b of undilute air through cloud base. The latter is determined according to the simple, elegant, and physically intuitive *subcloud-layer quasi-equilibrium hypothesis* (Raymond 1995), which states that convective mass fluxes will adjust so that air within the subcloud layer remains neutrally buoyant when displaced upward to *just above* the top of the subcloud layer. This is based on the idea that the timescale for surface fluxes and radiative cooling to destabilize the subcloud layer is relatively short. In the present implementation, we relax the cloud-base upward mass flux M_b toward subcloud-layer quasi equilibrium according to

$$\frac{\partial M_b}{\partial t} = \frac{\alpha}{\Delta t}(T_{\rho p} - T_\rho + \Delta T_k)_{\text{LCL}} - \frac{\mathcal{D}}{\Delta t}M_b, \qquad (2)$$

where α is a fixed parameter, $T_{\rho p}$ is the density temperature of a parcel lifted adiabatically from the subcloud layer, T_ρ is the environmental density temperature, and Δt the time step, which is used to normalize α and $\mathcal{D}$. A small damping effect is given by $\mathcal{D}$. The right-hand side of (2) is evaluated at the lifted condensation level (LCL). The LCL normally occurs between model levels, so (2) is evaluated by extrapolating the parcel density temperature upward from the first level below the LCL assuming a dry-adiabatic lapse rate, while the environmental density temperature is extrapolated downward from the first level above the LCL assuming a reversible moist-adiabatic lapse rate. In (2), ΔT_k is a specified temperature deficit at the LCL, which accounts for the ability of boundary layer turbulence to overcome negative buoyancy at the LCL. In principle, ΔT_k should be a function of the turbulence kinetic energy at the LCL, but here we take it to be constant. The effect of (2) is to adjust M_b so that $T_{\rho p} - T_\rho$ tends to remain constant.

As mentioned in the introduction, a primary concern in formulating a convective scheme for use in climate models is the microphysics. One is limited, on the other hand, by the fact that the clouds are parameterized and thus lack real spatial and temporal variability. Of principal concern is the fraction of condensed water that is converted to precipitation, as the remainder will contribute to moistening the environment. The two principal precipitation-forming processes in clouds are stochastic coalescence and the Bergeron–Findeisen mechanism. The efficiency with which stochastic coalescence forms precipitation is such a nonlinear function of the amount of cloud water that it is often represented as a step function of the cloud water content (Kessler 1969). Here we adopt that philosophy by converting all cloud water in excess of a threshold content, l_c, to precipitation within each sample of cloud air. Ice processes are crudely accounted for by allowing l_c to be temperature dependent:

$$l_c = \begin{cases} l_0 & T \geq 0°C \\ l_0\left(1 - \dfrac{T}{T_{\text{crit}}}\right) & T_{\text{crit}} < T < 0°C \\ 0 & T \leq T_{\text{crit}}, \end{cases} \qquad (3)$$

where l_0 is a warm cloud autoconversion threshold and T_{crit} is a critical temperature (°C) below which all cloud water is converted to precipitation.

While it is easy to be critical of a simple formulation like (3), it should be noted that it is similar to formulations used in some cloud models and, more importantly, that the three convective schemes most widely used in climate models make no attempt at all to account for the nonlinearity of stochastic coalescence.

In accounting for the disposition of precipitation once formed it is again necessary to make simplifications. One drastic simplification we make here is to *allow no interaction between cloud water and precipitation*. To be able to account for this, one must know something about the structure of clouds. For example, sloping updrafts of the kind often encountered in tropical squall lines (LeMone et al. 1984) may allow precipitation to fall out of the updraft before much interaction with cloud water can take place. In effect, we assume that most deep convection behaves in this way. A more sophisticated approach would account for the probable structure of convection by relating it to buoyancy and environmental shear, as has been done, for example, by Cheng and Arakawa (1997).

In the present scheme, the precipitation is added to a single, hydrostatic, unsaturated downdraft of assumed constant horizontal cross section. This downdraft transports heat and water substance, and precipitation evaporates according to a standard rate equation. Details of this formulation may be found in E91. We note here that it is necessary to assume that a specified fraction, σ_s, of the precipitation shaft falls through unperturbed environmental air and that the unsaturated downdraft occupies a specified fractional area, σ_d.

It was discovered in the process of evaluating the scheme that surface latent and sensible heat fluxes evaluated on the basis of array-scale winds were underestimated, roughly in proportion to the amount of convection in the array. This points to the important effects of deep convective downdrafts on surface fluxes, as documented rather thoroughly by Jabouille et al. (1996). Following those authors, we define a deep convective downdraft velocity scale, w_d, to be added to the wind speed used in surface flux formulations, according to

$$\overline{|\mathbf{V}|} = \sqrt{|\mathbf{V}|^2 + u^{*2} + w_d^2}, \qquad (4)$$

where $\overline{|\mathbf{V}|}$ may be considered a grid box–averaged surface wind speed, u^* is a (dry) turbulent boundary layer velocity scale, and w_d is a deep convective downdraft velocity scale. We take w_d to be proportional to the unsaturated downdraft mass flux, according to

TABLE 1. Parameters and their optimized values.

Parameter	Description	Optimized value
Λ	Mixing parameter	0.06 mb^{-1}
l_0	Warm-cloud autoconversion threshold	1.1 g kg^{-1}
T_{crit}	Critical temperature	$-55°C$
Omega_rain	Pressure fall speed of rain	50 P s^{-1}
Omega_snow	Pressure fall speed of snow	5.5 P s^{-1}
C_rain	Evaporation coefficient for rain	1.0
C_snow	Evaporation coefficient for snow	0.8
σ_d	Fractional area covered by downdraft	0.05
σ_s	Fraction of rain shaft falling through environment	0.15
ΔT_k	Convection buoyancy threshold	0.65 K
β	Downdraft surface velocity coefficient	10.0
α	Relaxation rate	0.02 kg m^{-2} s^{-1} K^{-1}
$\mathcal{D}$	Mass flux damping rate	0.01

$$w_d = \frac{\beta M_d}{\rho \sigma_d}, \qquad (5)$$

where β is a constant parameter, M_d is the unsaturated downdraft mass flux at cloud base, and ρ is the air density. As surface fluxes are quadratic quantities, averaging them over a grid box gives Reynolds-type correlation terms. In particular, for constant exchange coefficients, contributions of correlations between fluctuating wind speed and of temperature or specific humidity will have the form

$$-\overline{|\mathbf{V}|'x'},$$

where x is either temperature or specific humidity. We represent these terms in the convective scheme by

$$-w_d|x|', \qquad (6)$$

where $|x|'$ is an unsaturated downdraft temperature or specific humidity perturbation from the environment.

The scheme operates by checking each model level for instability to upward displacement (dry adiabatic followed by moist adiabatic), beginning at the lowest model level. For computational expedience, convection occurs only from the *first* model level that exhibits instability to upward displacement. Thus, while elevated convection can occur, it cannot do so when the boundary layer is also unstable. Observational evidence (e.g., Colman 1990) suggests that elevated convection generally happens when the boundary layer is decidedly stable.

Finally, the convection scheme rigorously conserves the vertically integrated enthalpy, satisfying the finite-difference equivalent of

$$\int_0^{p_0} \left\{ [C_{pd}(1 - q_t) + C_{pv}q_t]\left(\frac{\partial T}{\partial t}\right)_c + L_v\left(\frac{\partial q}{\partial t}\right)_c \right\} dp = 0,$$
$$(7)$$

where the integral is over the entire mass of the column (p_0 is the surface pressure); q_t is the total water content; C_{pd} and C_{pv} are the heat capacities at constant pressure of dry air and water vapor, respectively; L_v is the (temperature dependent) latent heat of vaporization; q is the specific humidity; and T the temperature. The partial derivations in (7) are tendencies owing to convection alone. In satisfying (7), all kinetic energy generated within convective clouds is assumed to be locally dissipated, ignoring advective and wave-related transport of energy away from convective clouds.

In summary, the convection scheme described here is based on E91 but differs from it in several important respects. Rates of mixing are based on a local entrainment hypothesis rather than, as in E91, global quasi-equilibrium, and the cloud-base mass flux is relaxed toward a state of boundary layer quasi equilibrium. Conversion of cloud to rain water is loosely based on a stochastic coalescence model, and unsaturated downdrafts are allowed to enhance surface fluxes. Finally, elevated convection is allowed, but not when the boundary layer is also unstable.

3. Evaluation

A sober reading of the previous section reveals a disturbing number of ad hoc assumptions and associated parameters. A list of all such parameters in the scheme is provided in Table 1, along with their optimum values, which have been arrived at by the means described later in this section. The number of ad hoc assumptions is large and greatly reduces the expectation that the scheme will perform well under a variety of circumstances. This will be a characteristic of virtually all schemes that purport to deal with microphysical issues; the parameter set can be reduced to a small number only by making sweeping assumptions. For example, one can use a single moisture partitioning parameter in Kuo-type schemes, but there is no physical basis behind such a partition. As another example, the original version of the Arakawa–Schubert (1974) scheme did not represent unsaturated, precipitation-driven downdrafts and thus avoided parameters dealing with the fall and evaporation of rain as well as the downdraft itself. But in so doing it omitted a major contribution to convective transports. The Betts (1986) scheme apparently contains only a single parameter governing the relaxation of the temperature and water vapor toward reference profiles, until

it is realized that the water vapor profile is entirely empirical, in which case one can think of the profile itself as containing one parameter for each model level. There is no physical basis for claiming universality of the water vapor profile.

From the work of Rennó et al. (1994) it is clear that the prediction of atmospheric water vapor is sensitive to assumptions about convective cloud microphysics. Given this observation and the large parameter sets associated with schemes that aim toward realism, there is a strong incentive to devise rigorous observational tests of the performance of the schemes. With the notable exception of the work of Betts and Miller (1986), such tests are almost entirely absent from the literature. It is more usual for convective schemes to be subjected to semiprognostic tests. In such tests, a single-column model containing the convective scheme is driven by forcing derived from an array of soundings, resulting in a prediction equation of the form

$$\frac{\partial x}{\partial t} = L_x + C_x, \tag{8}$$

where x is either temperature or specific humidity; C is the contribution by the convective scheme to the tendency of x; and L is the contribution by all other processes, including advection, surface fluxes, and radiation. We can write (8) equally well as

$$-C_x = L_x - \frac{\partial x}{\partial t}. \tag{9}$$

At a single time, the terms on the right can be evaluated from observations, while C_x is produced by the convection parameterization. The semiprognostic test simply compares the two. However, the test itself is essentially meaningless, simply because under most circumstances in which convection is active,

$$\frac{\left|\dfrac{\partial x}{\partial t}\right|}{|L_x|} \ll 1. \tag{10}$$

For example, actual temperature tendencies in the Tropics are of order 0.2 K day^{-1}, while convective heating can be of order 100 K day^{-1}. Thus, the right- and left-hand sides of (9) may appear to agree very well at the same time that $\partial x/\partial t$, which is what one really wants, is off by an order of magnitude or more. Nor is the disagreement of the two sides of (9) grounds for rejecting a convective scheme, because the resulting large time tendency may only last a few time steps in a prognostic model, as the profiles undergo a rapid but small adjustment; thereafter, the scheme may perform very well. For these reasons, semiprognostic tests are essentially useless for evaluating the performance of convective schemes.
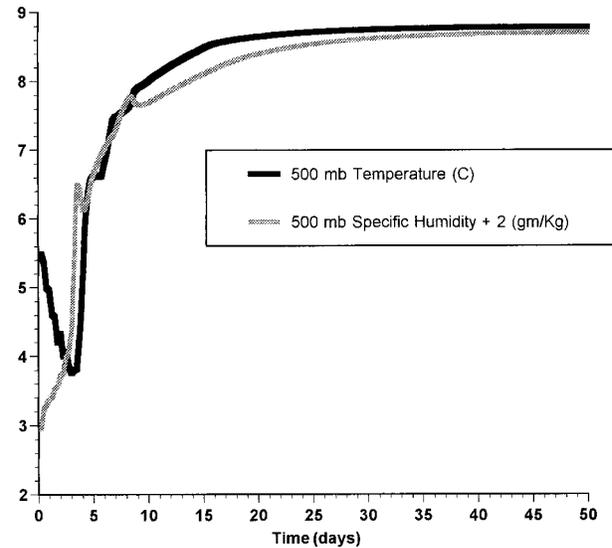

FIG. 2. Relaxation to radiative–convective equilibrium of temperature (dark) and specific humidity (light) from an arbitrary initial state. Single-column model is that of Rennó et al. (1994).

a. Technique

A better method was advocated by E91 and Randall et al. (1996) and has been used by Sud and Walker (1993). This consists of using (8) to make actual predictions of temperature and humidity over a period of time long enough for these quantities to reach statistical equilibrium. Figure 2 shows the adjustment of 500-mb temperature and specific humidity to a state of radiative-convective equilibrium, beginning with an arbitrary sounding, using the single-column model described by Rennó et al. (1994). Clearly, the adjustment time is of order 20 days. This timescale is set by the time necessary for a sample of air to subside through the troposphere under the influence of radiative cooling and illustrates a fundamental point about prediction of atmospheric properties in convecting regimes: adjustments of water vapor and temperature profiles depend critically on radiation, even when other processes dominate the heat and water budgets. This is because, in the clear air between clouds, the vertical velocity is always strongly constrained by the radiative cooling rate.

The prognostic, single-column test consists in integrating conservation equations for heat and moisture:

$$\frac{\partial T}{\partial t} + [\mathbf{V}_H \cdot \nabla T] + \left[\omega \frac{\partial T}{\partial p}\right] = \left[\frac{\alpha}{C_p'}\omega\right] + \left[g \frac{\partial \tau_T}{\partial p}\right]$$
$$+ [\dot{Q}_{\mathrm{rad}}] + F_T, \tag{11}$$

$$\frac{\partial q}{\partial t} + [\mathbf{V}_H \cdot \nabla q] + \left[\omega \frac{\partial q}{\partial p}\right] = \left[g \frac{\partial \tau_q}{\partial p}\right] + F_q, \tag{12}$$

where $\mathbf{V}_H$ is the horizontal vector velocity; ω is the pressure velocity; α is the specific volume; τ_T and τ_q are the dry convective turbulent fluxes of heat and mois-
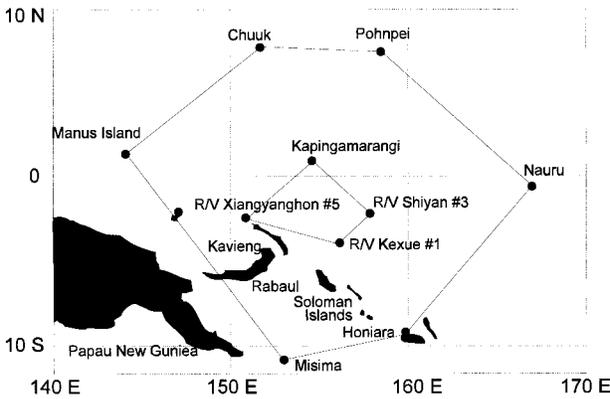
FIG. 3. Rawinsonde arrays in TOGA COARE. The solid dots represent rawinsonde stations. The inner array is the IFA.

ture, respectively; F_T and F_q are the moist convective tendencies of temperature and specific humidity; and $\dot{Q}_{rad}$ is the radiative heating rate. The moisture-weighted heat capacity at constant pressure is represented by C'_p, defined

$$C'_p \equiv C_{pd}(1 - q_t) + C_{pv}q_t.$$

The brackets in (11) and (12) denote terms that are, ideally, supplied on the basis of observations. It should be pointed out here that one may replace the vertical advection terms in (11) and (12) by

$$[\omega]\frac{\partial x}{\partial p},$$

where x is either temperature or specific humidity. In this variation, the observed vertical velocity acts on the predicted, rather than observed, vertical temperature gradient. Experiments with both formulations show differences, but no clear advantage of one over the other. We choose the form of (11)–(12) based on the relative simplicity of interpretation of a global enthalpy constraint, discussed presently.

b. Data

To evaluate the bracketed terms in (11) and (12) it is necessary to observe all three velocity components, temperature and specific humidity, radiative fluxes, and dry turbulent sensible and latent heat fluxes over a region large enough that the statistics of moist convective fluxes are well behaved. For the tests described here, we use data from the intensive flux array (IFA) operated in the western equatorial Pacific from 1 November 1992 to 28 February 1993 as part of the Tropical Ocean Global Atmosphere Couple Ocean–Atmosphere Research Experiment (TOGA COARE). The IFA is shown in Fig. 3. It is roughly 500 km across and thus meets the requirement of being much larger than typical intercloud length scales, though there were several instances in which convection within the IFA was dominated by a

single mesoscale convective system. A thorough description of weather in the IFA may be found in Veldon and Young (1994) and Lin and Johnson (1996). Note that soundings from the eastern and southern members of the array were taken only during three periods: 11 November to 11 December 1992; 18 December 1992 to 22 January 1993; and 31 January to 17 February 1993.

Rawinsonde soundings were taken every 6 h at the IFA stations shown in Fig. 3. These and other data sources were used to calculate the average temperature and specific humidity over the array as well as all the advective terms in (11) and (12). The pressure velocity ω was calculated from horizontal winds using mass continuity with a correction applied to force ω to vanish at 100 mb. Details of the procedure for estimating horizontal and vertical advections and ω over the IFA may be found in Lin and Johnson (1996).

Surface sensible and latent heat fluxes were derived every hour from moored buoys, as described by Weller and Anderson (1996). Dry turbulent fluxes in the subcloud layer were represented by a dry-adiabatic adjustment algorithm and it is assumed that dry turbulent fluxes are negligible above convective cloud base.

Radiative fluxes during TOGA COARE were observed only at the surface by moored buoys (Weller and Anderson 1996), and at the top of the atmosphere by satellite (Zhang et al. 1995; Rossow and Zhang 1995).[1] Thus, there are no direct observations that yield estimates of the vertical structure of the radiative heating of the atmosphere. To use (11) and (12) in a single-column model, either an assumption must be made about the structure of $\dot{Q}_{rad}$ or a radiative transfer code must be employed. We chose the former option in order to adhere most closely to the philosophy of using observations to estimate all the terms in (11) and (12) except those owing to convection. While there is much confidence in radiative transfer calculations in clear-sky conditions, the strong effects of clouds can only be represented parametrically in a single-column model, introducing another source of error. Using the observed surface and top of the atmosphere (TOA) radiative fluxes, one must make an assumption about the vertical distribution of the radiative heating rate. Here we simply assume that the radiative heating is uniformly distributed from the surface to 100 mb. While calculated radiative heating rates in the Tropics certainly show vertical structure, there is little net gradient from the surface to the tropopause. We assume that the stratosphere is in radiative equilibrium. Calculations using radiative transfer codes show that while such an assumption is warranted averaged over a diurnal cycle, net flux convergences in the middle and upper stratosphere, owing to ozone absorption, can be of order 10 W m^{-2} during the

---

[1] The albedos were reduced by 24% under the values used by Rossow and Zhang (1995) owing to their assumption of water-cloud optics.

daytime. The effect of neglecting this will be to exaggerate the diurnal cycle of radiative heating of the troposphere.

An important check on the quality of the data is made by forming a global enthalpy conservation equation from (11) and (12). Multiplying (11) by the moisture-weighted heat capacity C'_p and (12) by the (temperature-dependent) latent heat of vaporization L_v, adding the two results and integrating over the mass of the atmosphere gives

$$\frac{1}{g} \int_0^{p_0} \left[C'_p \left\{ \frac{\partial T}{\partial t} + [\mathbf{V}_H \cdot \boldsymbol{\nabla} T] + \left[\omega \frac{\partial T}{\partial p} \right] \right\} \right.$$

$$\left. - [\alpha\omega] + L_v \left\{ \frac{\partial q}{\partial t} + [\mathbf{V}_H \cdot \boldsymbol{\nabla} q] + \left[\omega \frac{\partial q}{\partial p} \right] \right\} \right] dp$$

$$= [F_{s_0}] + [F_{L_0}] + [I_0] - [I_{\text{TOA}}]. \qquad (13)$$

Here, F_{s_0} and F_{L_0} are the surface sensible and latent heat fluxes and I_0 and I_{TOA} are, respectively, the net upward radiative fluxes at the surface and at the top of the atmosphere.

Note that (13) does not involve the convective terms F_T of F_q, because convection cannot change the vertically integrated enthalpy. This is expressed by (7). With certain rearrangements, (13) may be regarded as a predictive equation for the vertically integrated enthalpy:

$$K \equiv \frac{1}{g} \int_0^{p_0} k \, dp, \qquad (14)$$

where k is the specific enthalpy,

$$k = C'_p T + L_v q.$$

The quantity K can be predicted using (13) and compared directly to observations with no input from the convection parameterization. Note also that only the radiative fluxes at the surface and the top of the atmosphere are needed and these are provided by the aforementioned observations.

Using the observations of the advections, surface fluxes, and surface and TOA radiation, (13) was integrated over the entire 120-day period of operation of the IFA. The predicted and observed values of k are compared in Fig. 4. At the end of the period, the predicted value of k is less than the observed value by the equivalent of a 25 K temperature error integrated over the troposphere, corresponding to an average error in the net energy input of 22 W m^{-2}. This is a serious error and it shows that *the predicted column enthalpy will have serious errors regardless of the performance of the convection scheme,* unless measures are taken to correct the data.

The source of this error could arise from several of the terms in (13). The horizontal advection terms can be ruled out, as they are very small. The vertical advection and adiabatic cooling terms are major contributors to the heat budget, and as the pressure velocities
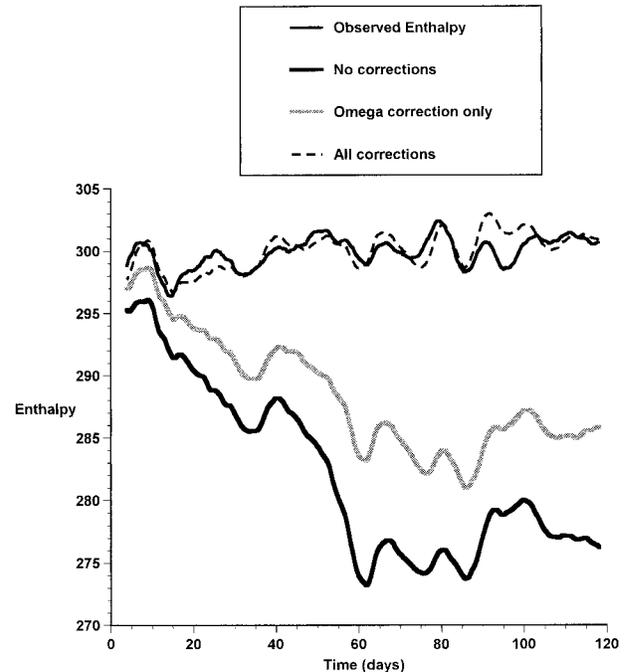

FIG. 4. Time evolution of vertically integrated enthalpy divided by $C_p \times 900$ mb, where C_p is the heat capacity at constant pressure. Units in K. Quantities have been smoothed by a 5-day running average. Thin dark line, observed; wide dark line, no corrections to observed forcing; wide light line, corrections to vertical velocities only; dashed line, all corrections applied. See text for explanation.

are calculated from horizontal mass divergence deduced from a limited set of rawinsondes, they are likely to contain significant errors. This may explain some systematic error in the ω's. Suppose, for example, that one or more rawinsonde stations have systematic errors in wind directions. This could lead to a systematic divergence error, given that wind directions are not uniformly distributed. But the systematic divergence error would lead to a systematic nonzero ω at the tropopause when the mass continuity equation is integrated upward from the surface. The algorithm used to force ω to zero at the tropopause would then eliminate the integrated divergence error. A systematic error could still contaminate the adjusted ω profile, though, if the systematic divergence error is not uniform with altitude. This scenario is illustrated in Fig. 5. Suppose that one boundary of an array is represented by a rawinsonde whose wind direction contains a systematic error and that the actual winds are southerly near the surface and northerly in the upper tropopause. Rotating these wind directions through a constant direction error may not affect the integrated divergence but will give a nonzero contribution to ω even after the adjustment to zero-integrated divergence has been made.

Errors in the calculation of surface and TOA radiation must also be accounted for. Measurements of the surface radiative fluxes by the IMET buoys (Weller and Anderson 1996) are thought to have errors of less than 10
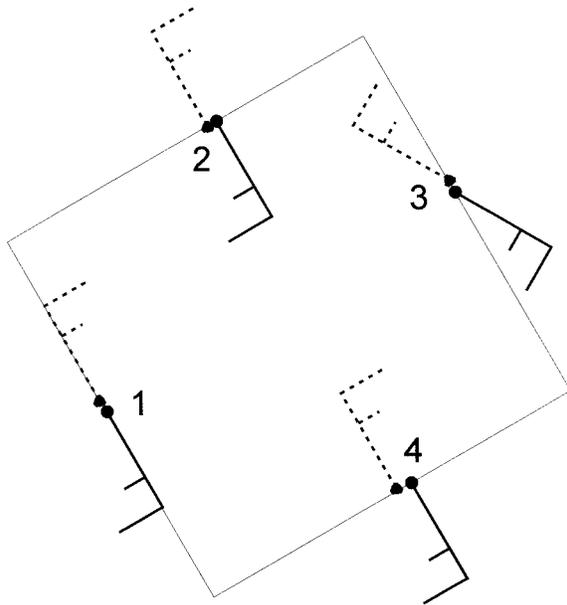
FIG. 5. Illustrates how systematic observation error can lead to systematic errors in vertical velocity. True wind is southeasterly at low levels and northwesterly aloft, indicated by the wind barbs at stations 1, 2, and 4. Station 3 has a systematic wind direction error.

FIG. 6. Observed latent heat flux (solid line) reported by Weller and Anderson (1996) and calculated latent heat flux (dashed). Units are W m^{-2}.

W m^{-2}. But there is a serious issue of how representative the buoy measurements are of the whole IFA area. While the large inhomogeneity of cloudiness may be expected to reduce this degree of representativeness, it is difficult to imagine how such difficulties could lead to systematic errors over 120 days.

If we were to assume that the entire 22 W m^{-2} error in the energy budget is because of some problem in the radiative fluxes and correct them accordingly, the average tropospheric temperature tendency owing to radiation would increase from about -0.7 to near -0.5 K day^{-1}.

Finally, the calculations of surface sensible and latent heat fluxes may involve some degree of error. The average sensible heat flux amounts to only about 10 W m^{-2}, so that errors in this estimate are unlikely to contribute significantly to the 22 W m^{-2} systematic error. The surface latent heat flux, on the other hand, averages close to 150 W m^{-2}, so that even a 10% underestimate may contribute significantly to the overall error. The surface fluxes were estimated using measurements of wind velocity, temperature, and specific humidity from the moored buoys.

Once again, the issue of representativeness of the fluxes arises, but it is not clear how undersampling might lead to a significant underestimate of the flux magnitude.

After a considerable amount of experimentation, the following procedure for enforcing enthalpy conservation was devised.

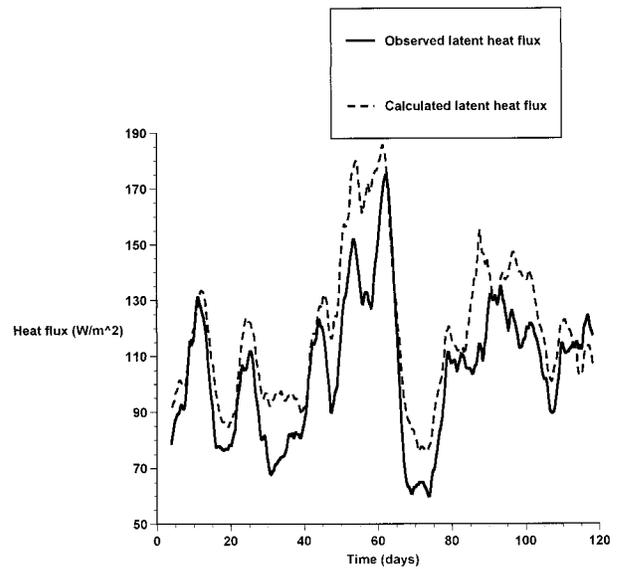First, at each rawinsonde observation time, each of the terms in (13) (including the time tendencies) was calculated using the aforementioned datasets, and the residual of the equation was obtained. Then the ω's were multiplied by a constant coefficient whose magnitude is such as to eliminate the residual. However, the magnitude of ω was not permitted to change by more than $\pm 50\%$. In practice, there were numerous instances where the adjustment coefficient reached this limit, leaving a still large residual in the tendencies.

The remaining residual was dealt with by smoothly relaxing the radiative flux divergence toward values that eliminate the remaining residual. This was done by adding terms to the tendencies of temperature in the troposphere, of the form

$$\left(\frac{\partial T}{\partial t}\right)_R = \frac{(k - k_p)}{\left(\frac{1}{g}\int_{p_t}^{p_0} C'_p \, dp\right)\tau_{\text{rad}}}, \qquad (15)$$

where k is defined by (14), k_p is the predicted value of k, and p_t is the tropopause pressure, here set to 100 mb. The temperature relaxation given by (15) is added only in the troposphere. The effect of (15) is to relax the predicted vertically integrated enthalpy back toward its observed value. We use a value of τ_{rad} of 5 days.

One other small change was made, partially as a means of testing and optimizing the interaction of the convection with surface fluxes, given by (4)–(6): we replaced the observed surface fluxes by those calculated using (4)–(6) with the IFA-averaged mean wind as input. The comparison between ''observed'' and calculated latent heat fluxes is shown in Fig. 6. On average, the calculated fluxes are larger than the observed.

The effects of these various adjustments on the global enthalpy budget are shown in Fig. 4. Correcting the ω's

alone results in only a small improvement to the budget, decreasing the integrated enthalpy error from the equivalent of 25 K to about 15 K. The radiative correction further reduces the error to nearly zero. (Note that these errors are not additive; if we introduce the radiative correction without the latent heat flux correction a much larger reduction in error—from 25 to 5 K—ensues.)

In summary, the raw forcing terms were altered to closely satisfy the global enthalpy constraint given by (13), which is independent of convection. The vertical velocities were altered at each observation time but the magnitude of the alteration was not permitted to exceed 50% of the raw value. Remaining residuals were dealt with by relaxing the tropospheric radiative cooling toward enthalpy-conserving values using (15). A considerable amount of subjective judgment was involved in arriving at this procedure; a more objective procedure awaits better error estimates for ω, surface fluxes, and radiation. Ideally, more integral constraints should be brought into play, following the methodology developed by Zhang and Lin (1997), but in this case the TOGA COARE dataset lacks high-quality area-integrated precipitation measurements necessary to constrain the moisture and heat budgets separately. This further illustrates the importance of obtaining high-quality precipitation datasets in sounding arrays used to optimize and evaluate convective parameterizations.

c. Parameter optimization

The preconditioned forcing was used to drive the single-column model, (11)–(12), using a vertical resolution of 25 mb. The prediction error was defined as the root-mean-square (rms) difference between the predicted and observed relative humidity:

$$E \equiv \left[\frac{1}{N} \sum (\mathcal{H}_p - \mathcal{H}_o)^2 \right]^{1/2}, \qquad (16)$$

where $\mathcal{H}_p$ and $\mathcal{H}_o$ are the predicted and observed relative humidities, N is the number of observations, and the sum is accumulated over each model time step and each model level up through 300 mb. (Observed relative humidities are considered unreliable above that level.) Observed humidities are interpolated between observation times.

Relative humidity was chosen for the error definition because, to a first approximation, it measures the effect of water vapor on radiative transfer, giving much more weight to fluctuations in the upper troposphere than would be the case if specific humidity were used. For radiative transfer, fluctuations of relative humidity in the upper troposphere are as important as those in the lower troposphere (Spencer and Braswell 1997).

Note that if the single-column model produces a good prediction of relative humidity, it is almost guaranteed to produce a good prediction of temperature owing to the global enthalpy constraint (13). This guarantees that

if the vertically integrated water content is correct, the vertically integrated temperature must also be correct. This still allows freedom for the vertical structure of temperature to differ from observations, but in convecting regions, the structure is strongly constrained to be close to that of a suitably defined moist adiabat (Betts 1982). For this reason, minimizing E in (16) should lead to a good prediction of temperature and thus no attempt was made to independently minimize the temperature error.

As an aid to finding the minimum value of E on a manifold whose dimensions are the parameter set given in Table 1, a linear tangent model (LTM) of the single-column model and its adjoint (ADJM) were written. The model adjoints have been widely used in applications of sensitivity theory to radiative–convective models (e.g., Hall 1986; Vukicevic and Errico 1993), and in parameter optimization theory (e.g., Tziperman and Thacker 1989; Wang et al. 1995). The models and their application used in this study are described in Zivkovic (1997).

Use of a model adjoint is advantageous since it provides a gradient of a model aspect of interest with respect to all model inputs during a single model run [see applications by Živković et al. (1995)]. In the present case, the model aspect of interest is rms error in relative humidity E, and the model input is a vector containing *all* the parameters, and initial and boundary conditions. The gradient of E (generally known as an objective function) with respect to model inputs provides the so-called adjoint sensitivities of the objective function with respect to each independent model input. For the purposes of parameter optimization, in this study we considered sensitivities involving model parameters only. The adjoint sensitivities of E with respect to parameters from Table 1 were calculated during independent monthly integrations with TOGA COARE data. They were used to aid finding the minimum value of E that produces optimal parameter values. The optimized parameter values are listed in Table 1, while the rms relative humidity and temperature errors remaining after optimization are 15.9% and 2.0 K, respectively. Given the myriad errors associated with the forcing data, it is not easy to deduce how much of this remaining error is related to data errors.

Figure 7 shows time–height sections of the difference between observed and predicted relative humidity and temperature, while Fig. 8 shows the same quantities averaged over the last 100 days of the 120-day period. The errors in both fields are concentrated on fairly short timescales. The time-averaged relative humidity (Fig. 8a) fits the observations quite well, except at the tropopause, where the single-column model predicts saturation. Observations of humidity at these temperatures (around $-70°C$) are not reliable, however. Virtually all mass-flux-type convective schemes produce saturation at the tropopause, where detrainment of water is not compensated for by subsidence. The time-averaged tem-
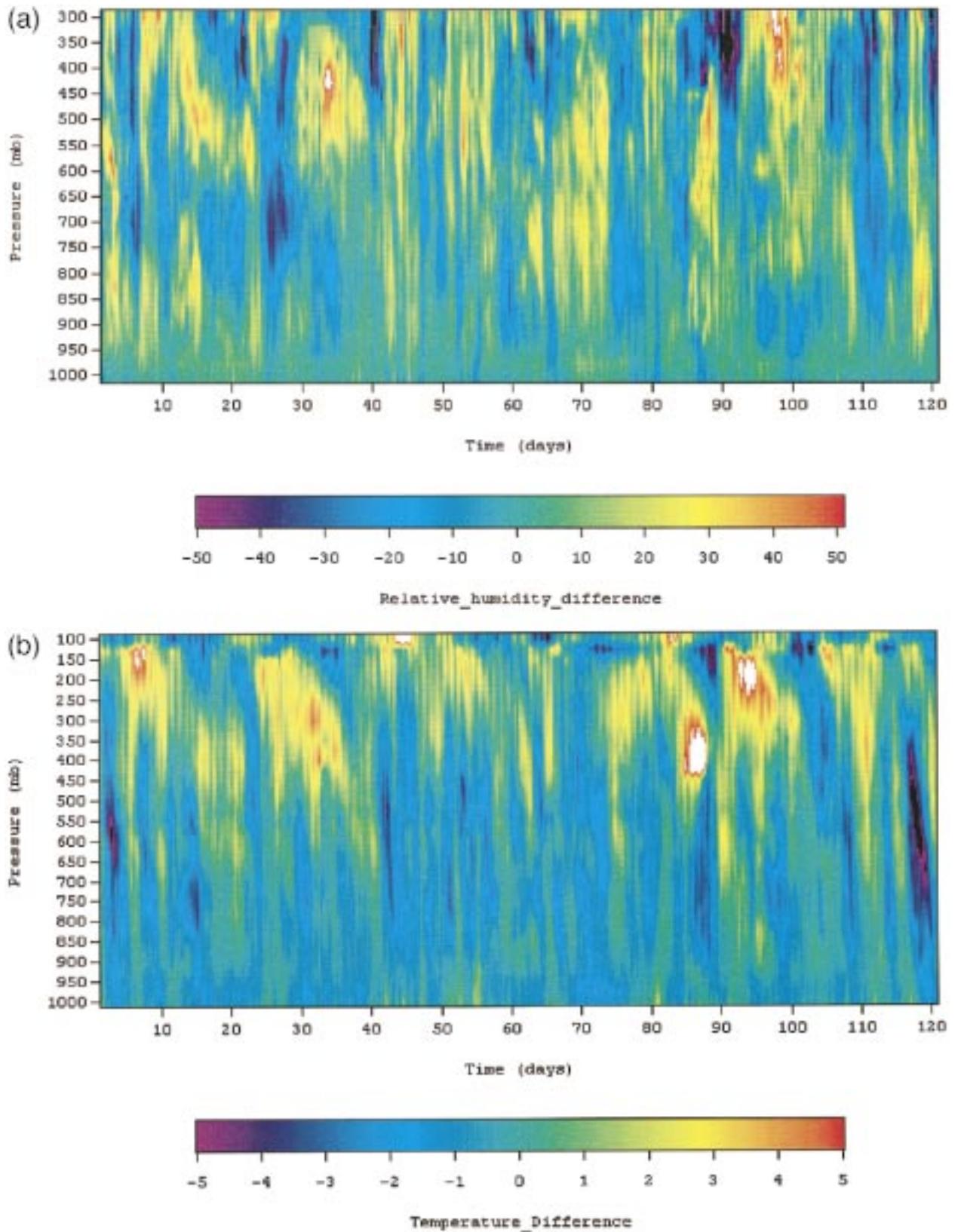
FIG. 7. Calculated minus observed (a) relative humidities (%) and (b) temperature (K) as a function of time and pressure, over the 120-day period of operation of the TOGA COARE IFA, using the optimized convective scheme.
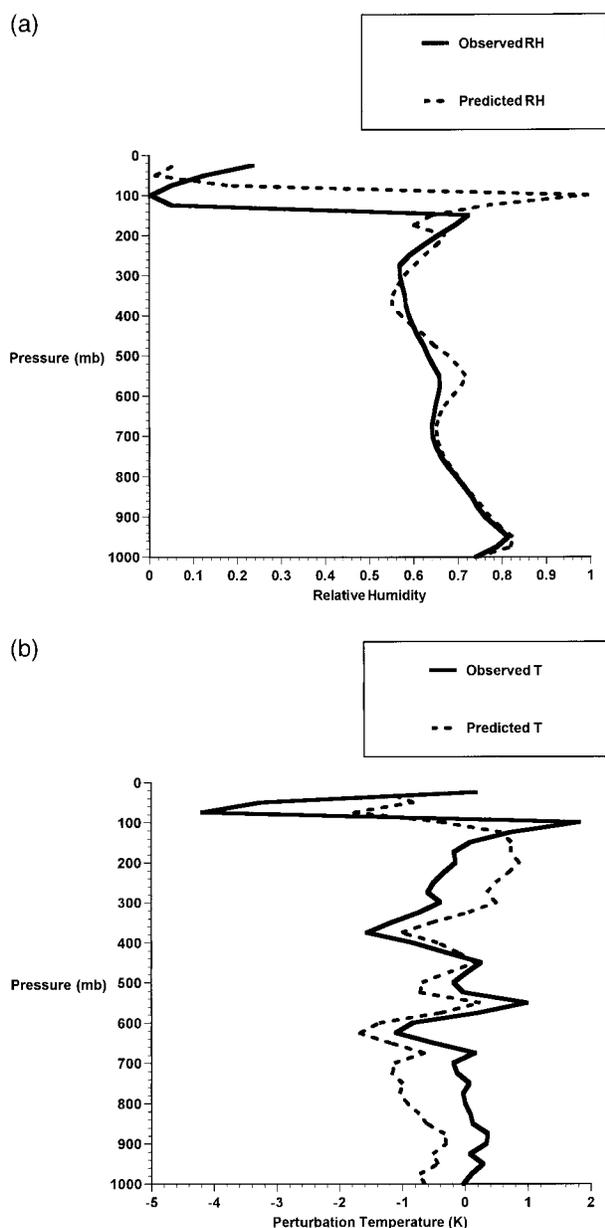
(a)

(b)

FIG. 8. Observed (solid) and predicted (dashed) relative humidity (a) and perturbation temperature (b) averaged over the last 100 days of operation of the TOGA COARE IFA. The perturbation temperature is the difference between the actual temperature and the temperature at the initial time.
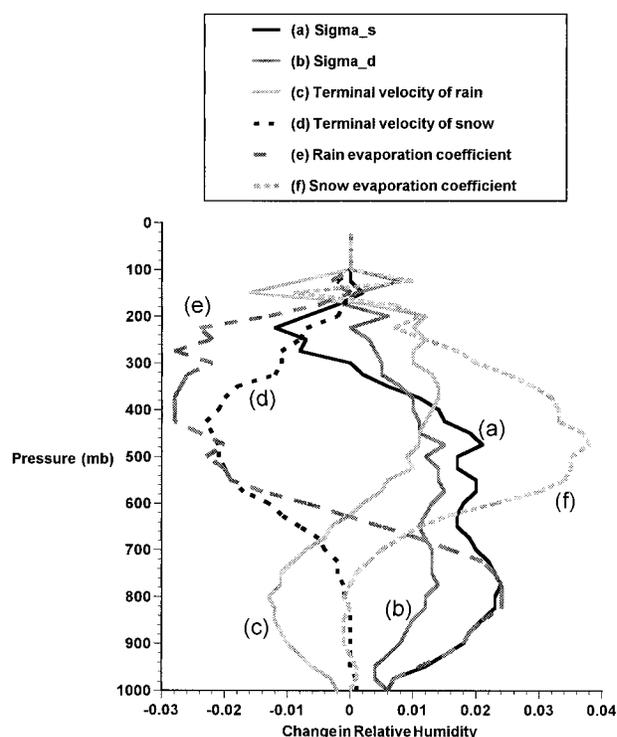

FIG. 9. Change in relative humidity from control experiment to experiments in which the indicated parameters are individually increased by 20%. The parameters varied are described in Table 1. Values represent averages over the last 100 days of operation of the TOGA COARE IFA.

perature perturbation (Fig. 8b) shows a systematic underestimation of the tropospheric lapse rate, by about 1 K over the depth of the troposphere.

That the prediction of relative humidity is sensitive to the microphysical parameters of the scheme is demonstrated in Fig. 9, which shows the time-averaged relative humidity that results when some of the key parameters are varied by 20% of their optimal magnitude. This confirms the sensitivity of relative humidity prediction to assumptions about cloud microphysics, discussed by Rennó et al. (1994).

d. Independent evaluation

The sensitivity of the relative humidity to the scheme's microphysical parameters, together with the guarantee of integrated enthalpy conservation, makes the optimization described here little more than an exercise in curve fitting. An objective evaluation of the scheme can be made by forcing it with completely independent data, preferably from a large number of different sounding arrays sampling very different convective regimes. Unfortunately, very few such datasets exist. As a first step in evaluating the performance of the optimized scheme, we force the single-column model using data collected during the Global Atmospheric Research Program Atlantic Tropical Experiment (GATE), conducted in the eastern tropical North Atlantic in 1974. The time evolution and all the advections of temperature and specific humidity were obtained from an archive maintained at Colorado State University and have been processed as described by Thompson et al. (1979). The vertical profile of radiative cooling was calculated by Cox and Griffith (1979) and represents an average over the 21 days of phase III of GATE. We did not account
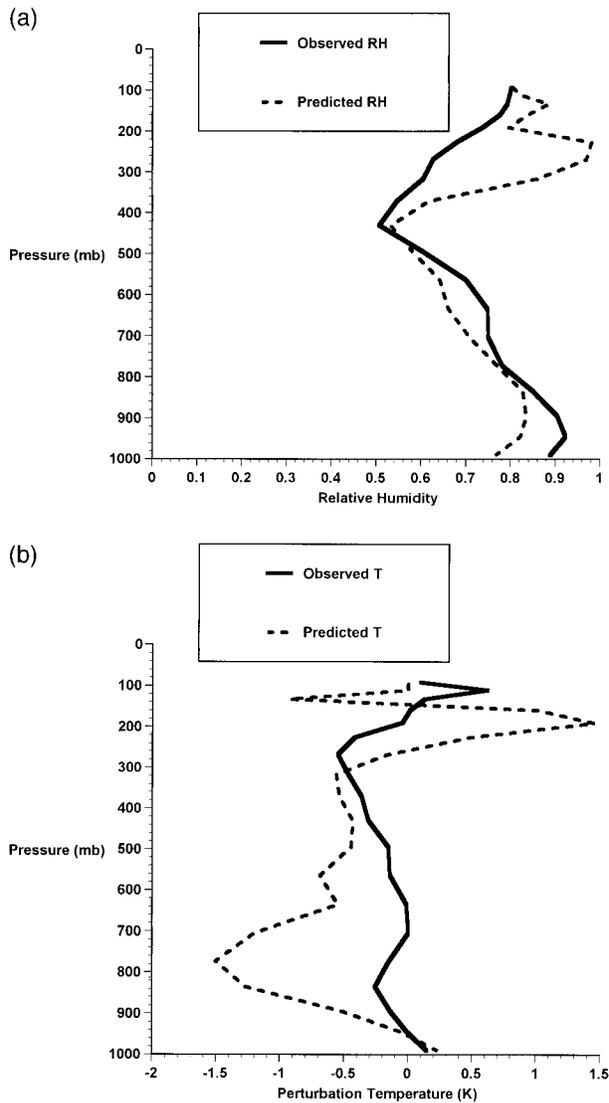
(a)

(b)

FIG. 10. Observed and predicted relative humidity (a) and perturbation temperature (b) averaged over the last 8 days of phase III of GATE. The perturbation temperature is the difference between the actual temperature and the temperature at the initial time.

for the variation of the radiative cooling profiles, nor did we attempt to correct the enthalpy budget terms as described previously for the TOGA COARE data.

The vertical profiles of temperature and humidity, averaged over the last 8 days of the period, are compared to the observed profiles in Fig. 10. The prediction is a little too dry in the lower troposphere and too moist above 400 mb. The temperature profile is too cold beneath the trade inversion and much too warm near the tropopause. Effectively, the model trade inversion is too strong by about 0.5°C and the lapse rate below the inversion is too steep by about 1.5°C. The root-mean-square relative humidity and temperature errors over the 21-day period are 15.26% and 1.43 K, respectively. These are comparable to the values found for the TOGA

COARE data, but in this case there is less time for the fields to drift away from their initial condition.

The comparison is encouraging, though problems are evident. Part of the problem may lie with the relatively coarse vertical resolution of the GATE dataset. While the TOGA COARE forcing data had a uniform vertical resolution of 25 mb, the GATE forcing was provided at irregular pressure intervals, with the largest values around 70 mb. The general effect of vertical resolution on humidity prediction will be explored presently.

e. Comparison with other convective schemes

As a means of further evaluating the new scheme, its performance is compared to that of three other convective schemes: the untuned, older version of this scheme (Emanuel 1991), the Betts–Miller–Janjic scheme (Janjic 1994), and a simplified Arakawa–Schubert scheme (Pan and Wu 1995). The last two schemes are versions currently in use in numerical weather prediction models operated by the National Centers for Environmental Prediction (NCEP). The Betts–Miller–Janjic scheme run by NCEP contains a number of significant modifications from the original Betts scheme (Betts 1986).

All schemes were incorporated in the single-column model described previously and forced using both the TOGA COARE IFA and GATE datasets. The same integrated enthalpy conservation measures were implemented as before for the TOGA dataset and, with the exception of the convection schemes themselves, all the models are identical.

Comparisons of the relative humidity predictions for GATE and TOGA COARE are shown in Figs. 11a and 11b, respectively. Not surprisingly, the present scheme outperforms the other three in the TOGA COARE comparison as it was specifically tuned to that dataset. The original version of this scheme is far too moist in the lower troposhere in both cases and, consistent with global enthalpy conservation, is too cold. It is also too dry in the upper troposphere in the GATE case. The Betts–Miller–Janjic scheme is too moist in the upper troposphere in both datasets and also in the lower troposphere in the TOGA COARE case. It performs quite well below 500 mb in the GATE case, but as with the present scheme, it is a little too dry in the lower troposphere in the GATE case. The Pan–Wu scheme is too dry in both cases above 600 mb and is also somewhat too dry in the lower troposphere above the subcloud layer in the TOGA COARE case. It performs as well as or better than the other schemes below 800 mb in the GATE case.

Comparisons between the predicted temperature perturbations from the initial state are shown for both datasets in Figs. 12a and 12b, respectively. All schemes are too cold below 500 mb in both datasets. The Pan–Wu scheme and the older version of the present scheme are much too cold in the GATE case. The present scheme and the Betts–Miller–Janjic scheme are remarkably similar above 600 mb in the GATE case. In the TOGA
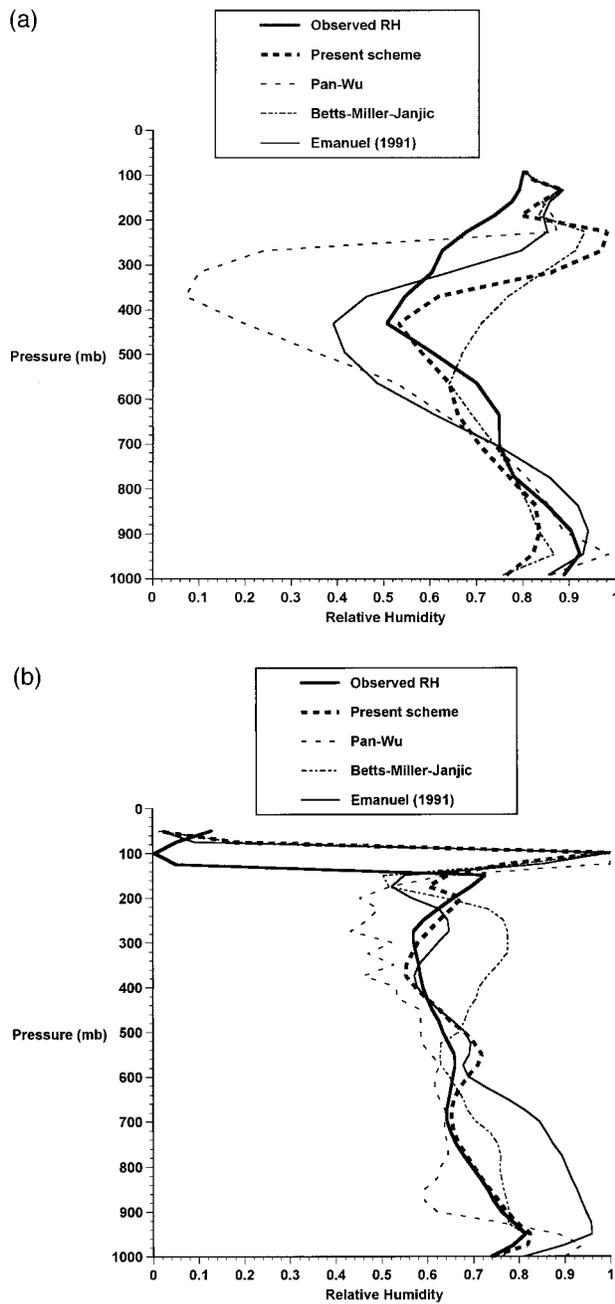
(a)

(b)

FIG. 11. Comparison between observed and predicted relative humidities for the present scheme, for the original version of the scheme (Emanuel 1991), and for the schemes of Pan–Wu (1995) and Janjic (1994). The fields averaged (a) over the last 8 days of GATE phase III and (b) for the last 100 days of the TOGA COARE IFA.

(a)

(b)

FIG. 12. Same as in Fig. 11 but for perturbation of temperature (K) from the initial state.

COARE case, there is a tendency for all schemes to produce tropospheric lapse rates whose magnitudes are too small. While it is difficult to pinpoint the cause of this, one might speculate that the assumption of vertically uniform radiative cooling in this case is at least partly to blame. Similarly, the radiative cooling pr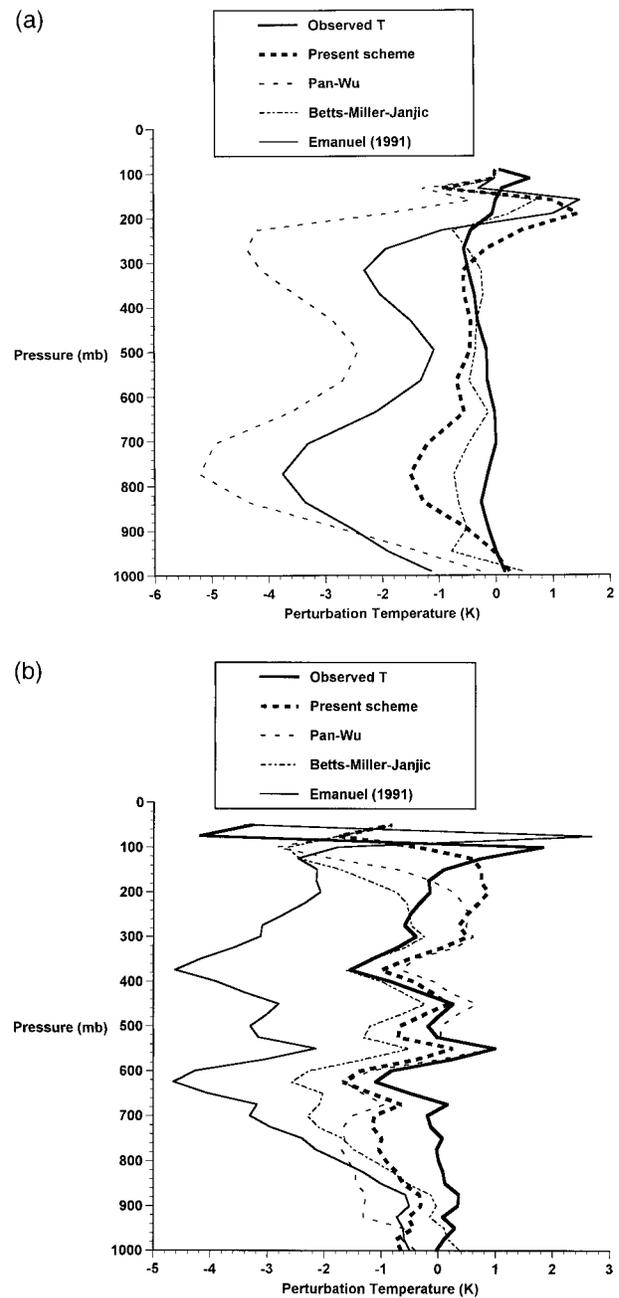ofiles used in the GATE case were calculated for clear-sky conditions and it is tempting to speculate that the absence of cirrus anvil cloud-top radiative cooling is partly responsible for the excessive warmth of the tropopause in the predictions using all the convection schemes.

The root-mean-square relative humidity and temperature errors over the entire time period and altitude range (up to and including 300 mb) are shown for each dataset in Tables 2 and 3, respectively. Not surprisingly, the present scheme outperforms the other three in the TOGA COARE case for which it was tuned. In the GATE case,

TABLE 2. Root-mean-square errors from TOGA COARE simulations, over last 100 days and up to 300 mb.

	Relative humidity (%)	Temperature (K)
Present scheme	15.94	2.00
Emanuel (1991)	21.68	4.56
Pan–Wu	22.31	3.16
Betts–Miller–Janjic	19.12	2.55

it outperforms the Pan–Wu scheme but is comparable to the Betts–Miller–Janjic scheme, whose original version was tuned to the GATE data (Betts and Miller 1986). But all of these comparisons are compromised to some degree by errors in the forcing and verification data, as indicated by the lack of global enthalpy conservation.

It is of some interest to compare the computational demands of the three schemes used here. For the 120 days of the TOGA COARE data, run with a 5-min time step on a Digital Equipment Corporation Alpha series workstation, the number of CPU seconds used by each scheme, in increasing order, were 43, 106, and 160 for the Betts–Miller–Janjic, present scheme, and Pan–Wu scheme, respectively. A small amount of this time in each case was used for input and output processing and physics other than convection. As one might have expected, the present scheme is not as fast as a relaxation scheme, like Betts–Miller, but faster than an Arakawa–Schubert-type scheme.

f. Effect of vertical resolution

The scale height of specific humidity in the atmosphere is about 3 km, so it stands to reason that vertical resolutions much better than 3 km will be necessary for accurate simulation of atmospheric water vapor. To explore the sensitivity of the humidity prediction to vertical resolution, we ran the single-column model at reduced resolution for the entire 120-day period of operation of the IFA. The results are displayed in Fig. 13. Reducing the vertical resolution from 25 to 50 mb clearly degrades the solution, especially just below the freezing level, where there is a large reduction of humidity. Further reduction of vertical resolution to 100 mb leads to large changes in predicted humidity, especially in the boundary layer and the upper troposphere, which becomes much too moist. The reduction of relative hu-

TABLE 3. Root-mean-square errors from GATE simulations, over last 8 days.

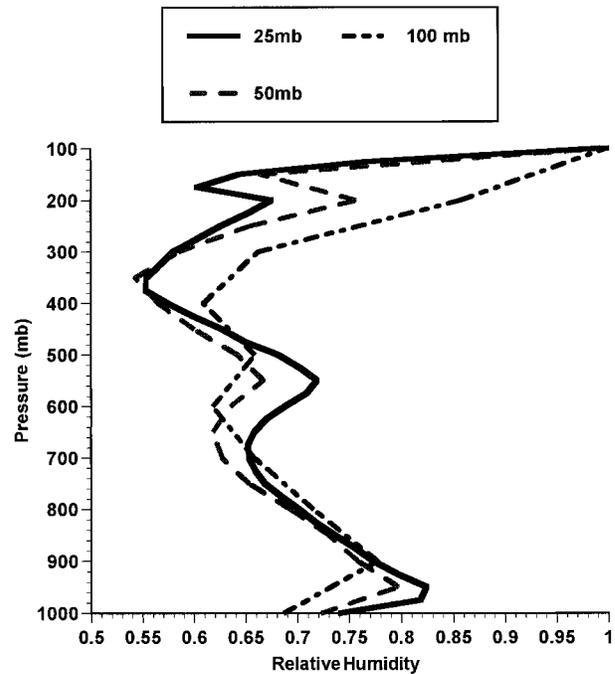|	Relative humidity (%)	Temperature (K)
Present scheme	15.26	1.43
Emanuel (1991)	15.88	2.34
Pan–Wu	24.77	2.93
Betts–Miller–Janjic	15.71	1.40

FIG. 13. The relative humidity averaged over the last 100 days of operation of the TOGA COARE IFA for the control run with 25-mb vertical grid spacing (solid), 50-mb spacing (dashed), and 100-mb spacing (dash–dot).

midity by 10% in the boundary layer may partially explain why experiments with the GATE data were too dry in the boundary layer (Fig. 11), given that the vertical resolution of the GATE data was comparatively poor.

Inadequate vertical resolution also masks the true sensitivity of the humidity prediction to cloud microphysics. To demonstrate this, we performed sensitivity experiments at both 25- and 100-mb resolutions. Figure 14 shows the difference between the relative humidity predictions over the 120-day period of the TOGA COARE IFA between the control experiment and an experiment in which the autoconversion threshold l_0 (see Table 1) was reduced to zero. As expected, the increased conversion of cloud water to precipitation dries the atmosphere by an average of 6% in relative humidity, but when the vertical resolution is degraded to 100 mb, the average reduction is only around 1.5%. Thus, *the sensitivity to cloud microphysics is greatly reduced at vertical resolutions comparable to those used in typical climate models.* This may explain why the water vapor feedback factors in climate models are all quite similar in spite of the use of a large variety of convective schemes (Cess et al. 1990). The lack of numerical resolution of water vapor is probably also responsible for the large and artificial vertical coherence of fluctuations of relative humidity in climate models, shown by Sun and Oort (1995).
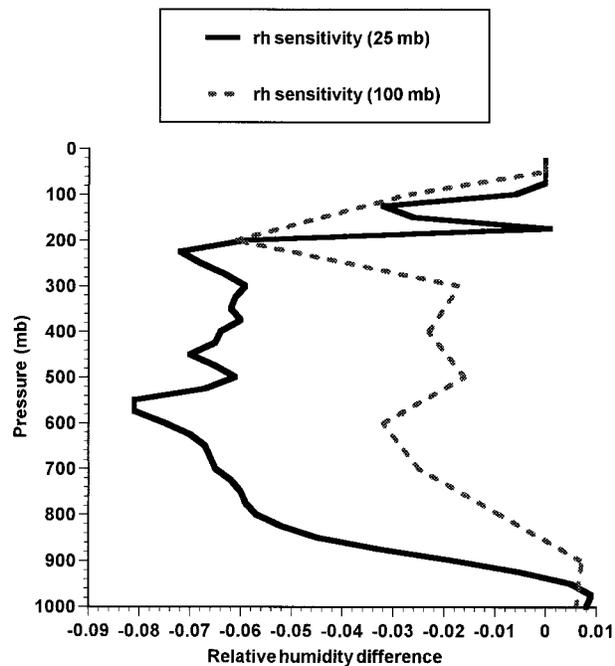
FIG. 14. Relative humidity difference from the control for simulations in which the autoconversion threshold (l_0; Table 1) has been reduced to zero, for 25-mb (solid) and 100-mb (dashed) vertical resolutions.

4. Summary

We have described an updated representation of cumulus convection that attempts to represent in a physically realistic way the physics of entrainment and mixing, cloud microphysical processes, and large-scale control of ensemble convective activity, emphasizing as well the importance of the interaction between convective downdrafts and surface fluxes. Using the TOGA COARE IFA dataset, we adjusted the parameters of the scheme to optimize the prediction of relative humidity over the last 100 days of the 120-day period. The optimized scheme was then evaluated using the GATE phase III data and compared to the performance of two different convection schemes. Finally, we attempted to quantify the rather large effects of vertical resolution on the performance of the single-column model. We emphasize the following conclusions from this work.

- Any reasonable attempt to include realistic cloud microphysics in a representation of convection will necessarily lead to a proliferation of parameters of uncertain value (e.g., Table 1). Climate prediction will be sensitive to the values of such parameters, as shown by Rennó et al. (1994). While such sensitivity may be exaggerated in single-column models, basic physical reasoning shows that climate in the real world will remain sensitive to assumptions about convective cloud microphysics.
- In seeming contradiction to the previous point, most climate models show relatively small sensitivity of

water vapor feedback to the type of convection scheme used. We here show that the small sensitivity of climate model water vapor feedback to the convection scheme is very likely owing to inadequate vertical resolution, as also documented by Sun and Oort (1995).

- The sensitivity of climate to convective cloud physics makes it imperative that convection schemes be subjected to rigorous tests designed to isolate their flaws. We argue that, owing to the relatively long adjustment time for water vapor, fully prognostic tests with observed forcing must be carried out over periods of at least 20–30 days.
- The data used to force single-column models must be examined carefully for energetic consistency. In particular, the data must be conditioned to ensure global enthalpy conservation, which is independent of convection. Failure to ensure such conservation may lead to false conclusions about the performance of convection schemes.
- The data used to optimize a scheme must not be used to evaluate it. Rigorous evaluation of convective scheme performance is currently impeded by the small number of suitable sounding array datasets and by poor measurement of humidity in the upper troposphere.
- The scheme developed here performs comparably to or better than three others in its predictions of temperature and humidity evolution using the GATE data, but further evaluation is needed. This must await the advent of high-quality sounding arrays operated for periods of many weeks or greater.

Given the problems inherent in using real observations to force single-column models, it would be nice to use forcing from limited regions within cloud-resolving models. We plan to carry out such tests in the near future.

REFERENCES

Arakawa, A., and W. H. Schubert, 1974: Interaction of a cumulus cloud ensemble with the large-scale environment, Part I. *J. Atmos. Sci.,* **31,** 674–701.

Betts, A. K., 1982: Saturation point analysis of moist convective overturning. *J. Atmos. Sci.,* **39,** 1484–1505.

——, 1986: A new convective adjustment scheme. Part I: Observational and theoretical basis. *Quart. J. Roy. Meteor. Soc.,* **112,** 677–691.

——, and M. J. Miller, 1986: A new convective adjustment scheme. Part II: Single column tests using GATE wave, BOMEX, ATEX and arctic air-mass data sets. *Quart. J. Roy. Meteor. Soc.,* **112,** 693–709.

Bretherton, C. S., and P. K. Smolarkiewicz, 1989: Gravity waves, compensating subsidence, and detrainment around cumulus clouds. *J. Atmos. Sci.,* **46,** 740–759.

Carpenter, R. L., Jr., K. K. Droegemeier, and A. M. Blyth, 1998: Entrainment and detrainment in numerically simulated cumulus congestus clouds. Part I: General results. *J. Atmos. Sci.,* **55,** 3417–3432.

Cess, R. D., and Coauthors, 1990: Intercomparison and interpretation of climate feedback processes in 19 atmospheric general circulation models. *J. Geophys. Res.,* **95,** 16 601–16 615.

Cheng, M.-D., and A. Arakawa, 1997: Inclusion of rainwater budget and convective downdrafts in the Arakawa–Schubert cumulus parameterization. *J. Atmos. Sci.,* **54,** 1359–1378.

Colman, B. R., 1990: Thunderstorms above frontal surfaces in environments without positive CAPE. Part I: A climatology. *Mon. Wea. Rev.,* **118,** 1103–1121.

Cox, S. K., and K. T. Griffith, 1979: Estimates of radiative divergence during Phase III of the GARP Atlantic Tropical Experiment. Part II: Analysis of Phase III results. *J. Atmos. Sci.,* **36,** 586–601.

Emanuel, K. A., 1991: A scheme for representing cumulus convection in large-scale models. *J. Atmos. Sci.,* **48,** 2313–2335.

——, and R. T. Pierrehumbert, 1996: Microphysical and dynamical control of tropospheric water vapor. *Clouds, Chemistry and Climate,* P. J. Crutzen and V. Ramanathan, Eds., Springer-Verlag, 264 pp.

Gyakum, J. R., and Coauthors, 1996: A regional model intercomparison using a case of explosive oceanic cyclogenesis. *Wea. Forecasting,* **11,** 521–543.

Hall, M. C. G., 1986: Application of adjoint sensitivity theory to an atmospheric general circulation model. *J. Atmos. Sci.,* **43,** 2644–2651.

Jabouille, P., J. L. Redelsperger, and J. P. LaFore, 1996: Modification of surface fluxes by atmospheric convection in the TOGA COARE region. *Mon. Wea. Rev.,* **124,** 816–837.

Janjic, Z. I., 1994: The step-mountain eta coordinate model: Further developments of the convection, viscous sublayer, and turbulence closure schemes. *Mon. Wea. Rev.,* **122,** 927–945.

Kessler, E., 1969: *On the Distribution and Continuity of Water Substance in Atmospheric Circulation.* Amer. Meteor. Soc., 84 pp.

Kuo, H.-L., 1974: Further studies of the parameterization of the influence of cumulus convection on large-scale flow. *J. Atmos. Sci.,* **31,** 1232–1240.

LeMone, M. A., G. M. Barnes, E. J. Szoke, and E. J. Zipser, 1984: The tilt of the leading edge of mesoscale tropical convective lines. *Mon. Wea. Rev.,* **112,** 510–519.

Lin, X., and R. H. Johnson, 1996: Kinematic and thermodynamic characteristics of the flow over the western Pacific warm pool during TOGA COARE. *J. Atmos. Sci.,* **53,** 695–715.

Lindzen, R. S., 1990: Some coolness concerning global warming. *Bull. Amer. Meteor. Soc.,* **71,** 288–299.

Manabe, S., J. Smagorinsky, and R. F. Strickler, 1965: Simulated climatology of a general circulation model with a hydrologic cycle. *Mon. Wea. Rev.,* **93,** 769–798.

Pan, H.-L., and W.-S. Wu, 1995: Implementing a mass flux convection parameterization package for the NMC Medium-Range Forecast Model. NMC Office Note 409, 40 pp. [Available form the National Centers for Environmental Prediction, Stop 9910, 4700 Silver Hill Road, Washington, DC 20233-9910.]

Pierrehumbert, R. T., and H. Yang, 1993: Global chaotic mixing on isentropic surfaces. *J. Atmos. Sci.,* **50,** 2462–2480.

Randall, D. A., K.-M. Xu, R. J. C. Somerville, and S. Iacobellis, 1996: Single-column models and cloud ensemble models as links between observations and climate models. *J. Climate,* **9,** 1683–1697.

Raymond, D. J., 1995: Regulation of moist convection over the west Pacific warm pool. *J. Atmos. Sci.,* **52,** 3945–3959.

——, and A. M. Blyth, 1986: A stochastic model for nonprecipitating cumulus clouds. *J. Atmos. Sci.,* **43,** 2708–2718.

Rennó, N. O., K. A. Emanuel, and P. H. Stone, 1994: Radiative-convective model with an explicit hydrological cycle. 1: Formulation and sensitivity to model parameters. *J. Geophys. Res.,* **99,** 14 429–14 441.

Rossow, W. B., and Y.-C. Zhang, 1995: Calculation of surface and top of atmosphere radiative fluxes from physical quantities based on ISCCP data sets. 2: Validation and first results. *J. Geophys. Res.,* **100,** 1167–1197.

Spencer, R. W., and W. D. Braswell, 1997: How dry is the tropical free troposphere? Implications for global warming theory. *Bull. Amer. Meteor. Soc.,* **78,** 1097–1106.

Sud, Y. C., and G. K. Walker, 1993: A rain evaporation and downdraft parameterization to complement a cumulus updraft scheme and its evaluation using GATE data. *Mon. Wea. Rev.,* **121,** 3019–3039.

Sun, D.-Z., and A. H. Oort, 1995: Humidity–temperature relationships in the tropical troposphere. *J. Climate,* **8,** 1974–1987.

Taylor, G. R., and M. B. Baker, 1991: Entrainment and detrainment in cumulus clouds. *J. Atmos. Sci.,* **48,** 112–121.

Thompson, R. M., Jr., S. W. Payne, E. E. Recker, and R. J. Reed, 1979: Structure and properties of synoptic-scale wave disturbances in the intertropical convergence zone of the eastern Atlantic. *J. Atmos. Sci.,* **36,** 53–72.

Tziperman, E., and W. C. Thacker, 1989: An optimal-control/adjoint-equations approach to studying the oceanic general circulation. *J. Phys. Oceanogr.,* **19,** 1471–1485.

Velden, C. S., and J. A. Young, 1994: Satellite observations during TOGA COARE: Large-scale descriptive overview. *Mon. Wea. Rev.,* **122,** 2426–2441.

Vukicevic, T., and R. M. Errico, 1993: Linearization and adjoint of parameterized moist diabatic processes. *Tellus,* **45A,** 493–510.

Wang, Z. I., M. Navon, X. Zou, and F. X. Le Dimet, 1995: A truncated Newton Optimization algorithm in meteorology applications with analytic Hessian/vector products. *Comput. Optim. Appl.,* **4,** 241–262.

Warner, J., 1970: On steady-state one-dimensional models of cumulus convection. *J. Atmos. Sci.,* **27,** 1035–1040.

Wei, D., A. M. Blyth, and D. J. Raymond, 1998: Buoyancy of convective clouds in TOGA COARE. *J. Atmos. Sci.,* **55,** 3381–3391.

Weller, R. A., and S. P. Anderson, 1996: Surface meteorology and air–sea fluxes in the western equatorial Pacific warm pool during TOGA Coupled Ocean–Atmosphere Response Experiment. *J. Climate,* **9,** 1959–1990.

Zhang, M. H., and J. L. Lin, 1997: Constrained variational analysis of sounding data based on column-integrated budgets of mass, heat, moisture, and momentum: Approach and application to ARM measurements. *J. Atmos. Sci.,* **54,** 1503–1524.

Zhang, Y.-C., W. B. Rossow, and A. A. Lacis, 1995: Calculation of surface and top of atmosphere radiative fluxes from physical quantities based on ISCCP data sets. 1: Method and sensitivity to input data uncertainties. *J. Geophys. Res.,* **100,** 1149–1165.

Živković, M., 1997: Variational optimization of sub-grid scale convection parameters. Final Report, Department of Energy, 58 pp. [Available from Atmospheric and Environmental Research, 840 Memorial Drive, Cambridge, MA 02139.]

——, J.-F. Louis, and J.-L. Moncet, 1995: Sensitivity analysis of a radiation parameterization. *J. Geophys. Res.,* **100** (D7), 13 827–13 840.